Electronic Supporting Information

Osmotic Pressure-Induced Pocket–Like Spheres with Fe Single–Atom Sites for Oxygen Reduction Reaction

Kuang Liang,[a] Chengzong Yuan,[b] Xiao Zhou, [b] Zhengkun Yang, [b] Junyi Du, [b] Yifan Ye,[c] Jingjing Luo,[a] Cai Chen, [b] Junfa Zhu,[c] Chenliang Su*[a] and Yuen Wu*[b,d]

[a]Address here. International Collaborative Laboratory of 2D Materials for Optoelectronic Science & Technology, Engineering Technology Research Center for 2D Materials Information Functional Devices and Systems of Guangdong Province, Institute of Microscale Optoelectronics, Shenzhen University, Shen Zhen 518060, China, E-mail: chmsuc@szu.edu.cn
[b]Hefei National Laboratory for Physical Sciences at the Microscale, School of Chemistry and Materials Science, University of Science and Technology of China, Hefei 230026, China, E-mail: yuenwu@ustc.edu.cn
[c]National Synchrotron Radiation Laboratory, University of Science and Technology of China, Hefei 230029, China
[d]Dalian National Laboratory for Clean Energy, Dalian 116023, China

Additional Figures and Tables

Fig. S1 Scheme of the formation of the Fe/NC(SS) catalyst.

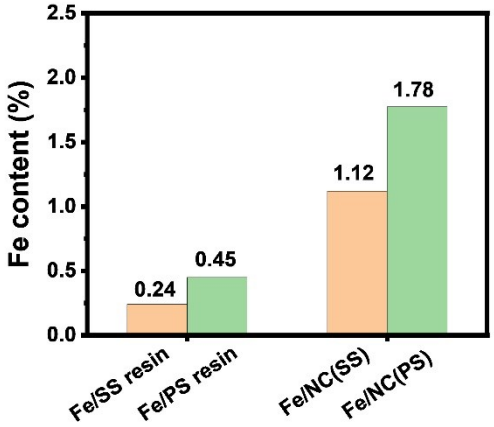

Fig. S2 Fe content by ICP–MS measurements of Fe/NC(SS) and Fe/NC(PS), comparing with their precursors of Fe/SS resin and Fe/PS resin.

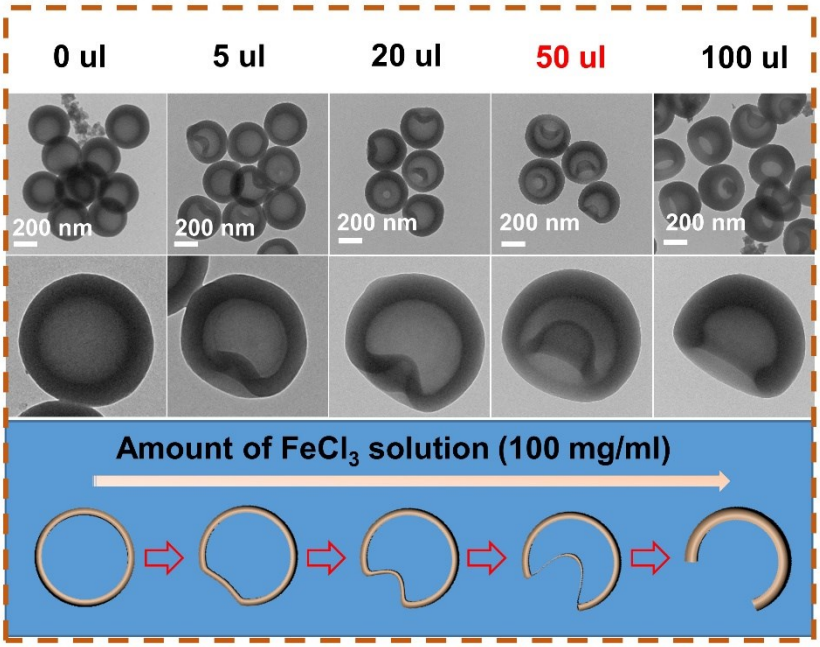

Fig. S3 Morphology changes with the gradually increasing usage of $FeCl_3$ (200 mg/ml). When the usage of $FeCl_3$ solution increases from 5 ul to 100 ul, the pocket sizes also grow.

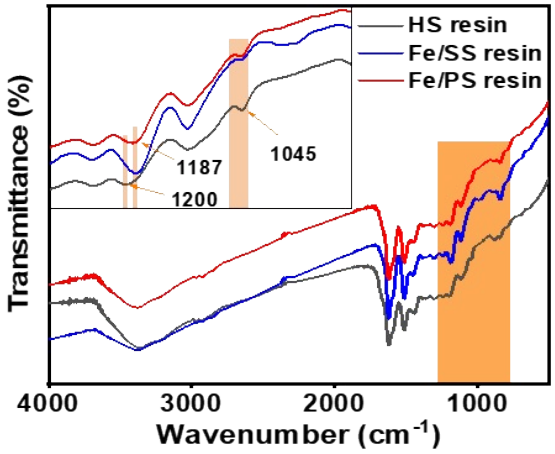

Fig. S4 FITR spectra analysis of the precursors: HS resin, Fe/SS resin, and Fe/PS resin. The insert displays the zoom–in curves in the orange range.

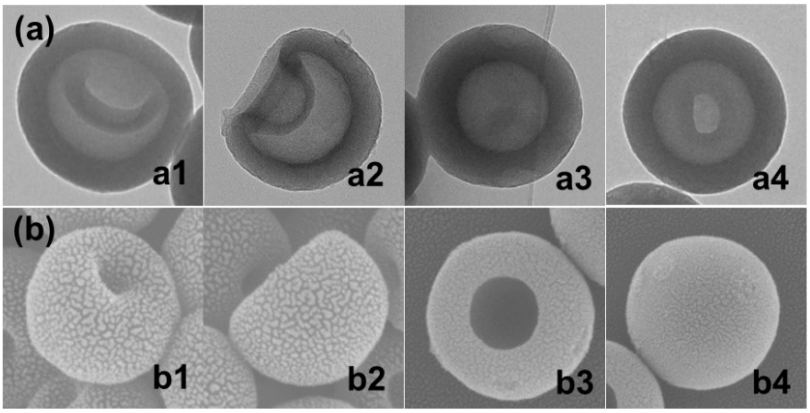

Fig. S5 TEM (a) and SEM (b) images of Fe/NC(PS) from the different viewing angles.

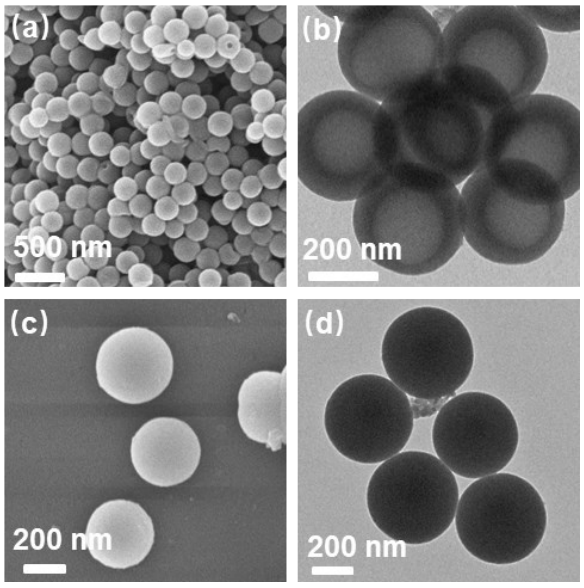

Fig. S6 SEM (a) and TEM (b) images of HS, SEM (c) and TEM (d) images of Fe/NC(SS).

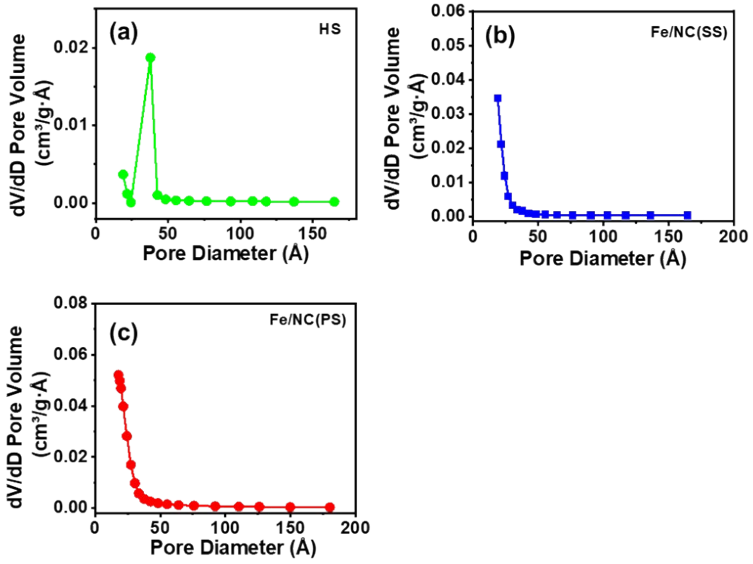

Fig. S7 The pore distribution of HS, Fe/NC(SS), and Fe/NC(PS).

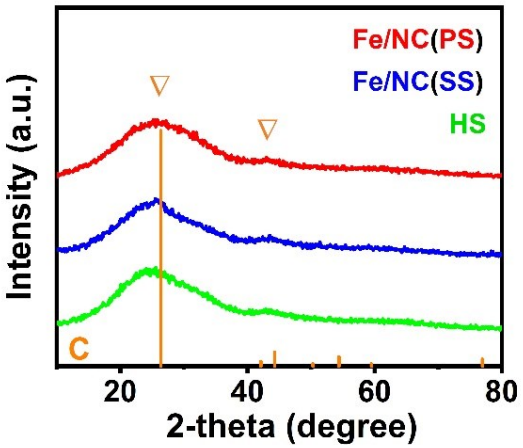

Fig. S8 XRD patterns of HS, Fe/NC(SS), and Fe/NC(PS).

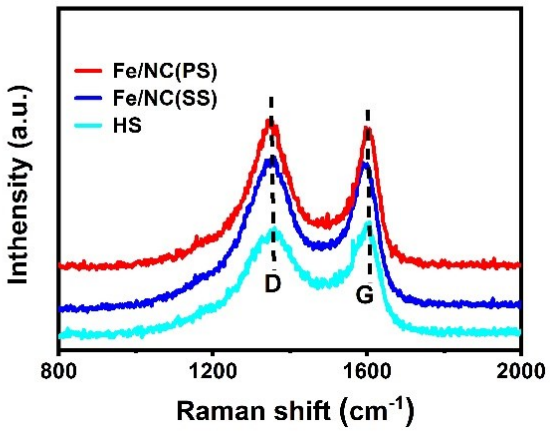

Fig. S9 Raman spectra of HS, Fe/NC(SS), and Fe/NC(PS).

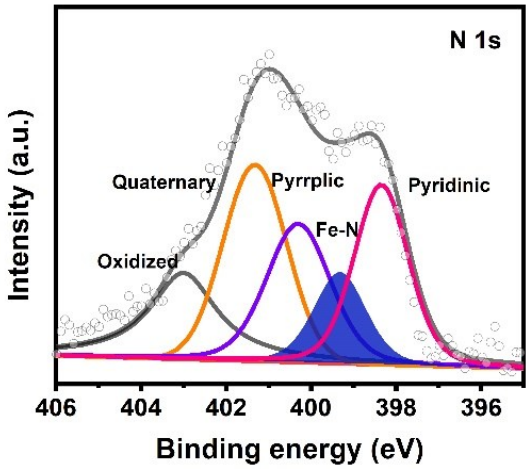

Fig. S10 High–resolution XPS spectrum for the N 1s in Fe/NC(PS).

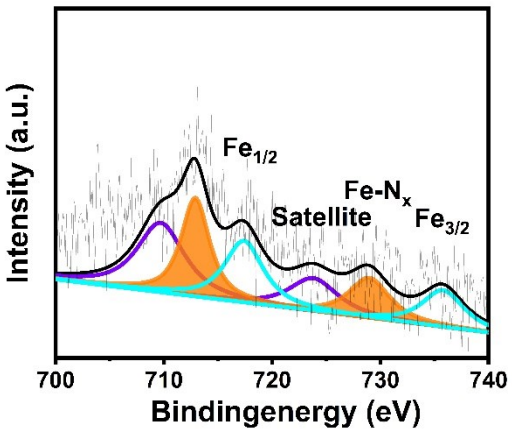

Fig. S11 High–resolution XPS spectrum for the Fe 2p in Fe/NC(PS).

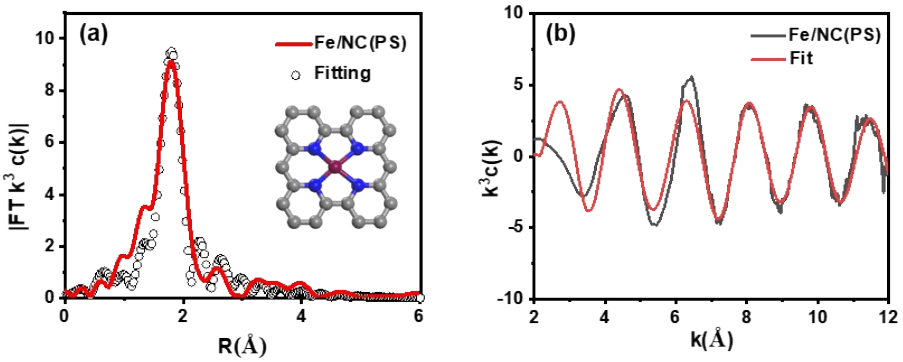

Fig. S12 (a) FT–EXAFS fitting curve of Fe/NC(PS) sample. Inset: atomic structure model of Fe/NC(PS), Fe (red), N (blue), and C (gray). (b) The corresponding EXAFS and k space fitting curves of Fe/NC(PS).

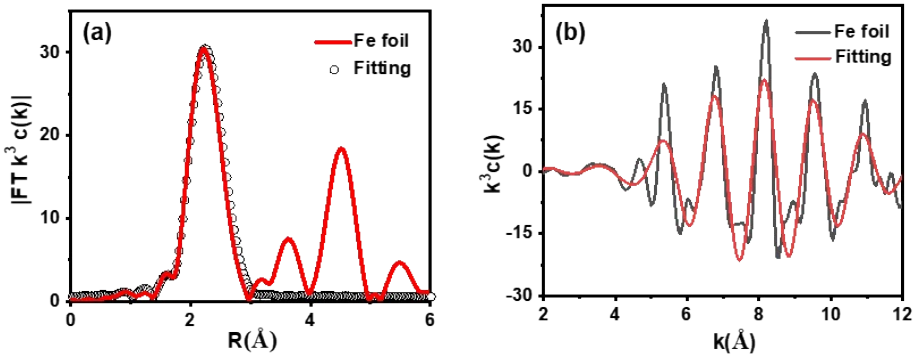

Fig. S13 The corresponding EXAFS fitting curves of Fe foil.

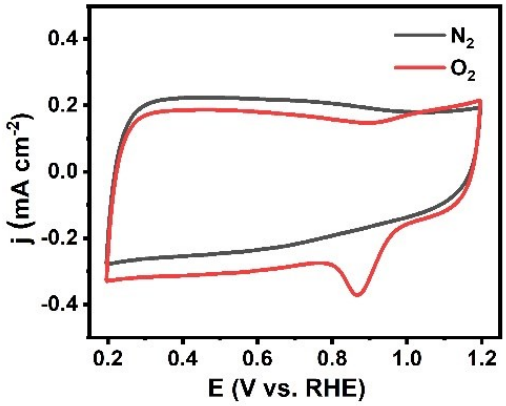

Fig. S14 CV curves in N_2/O_2–saturated 0.1 M KOH solution at a scan rate of 50 mV s^{-1}.

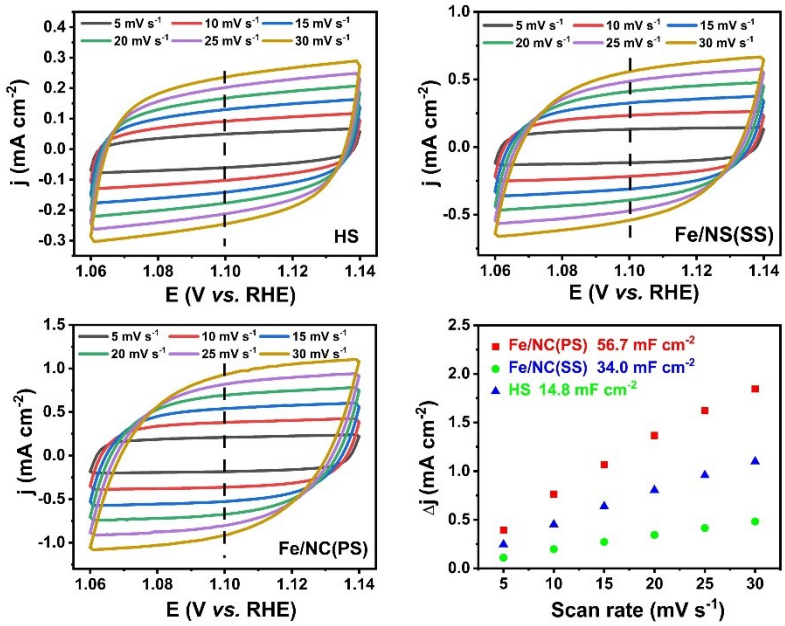

Fig. S15 Non-Faradic double layer capacitance measurements. a-c, CV curves at different scan rates for commercial HS, Fe/NC(SS), and Fe/NC(PS), respectively. d, Capacitive Δj = ja − jc as a function of the scan rate of catalysts.

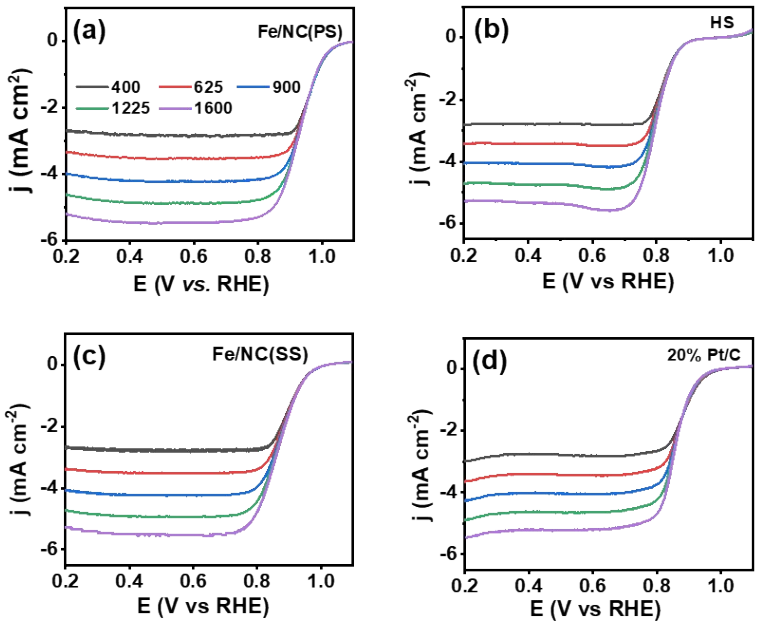

Fig. S16 LSV curves of different catalysts at varying rotation rates. (a) Fe/NC(PS), (b) HS, (c) Fe/NC(SS) and (d) Pt/C.

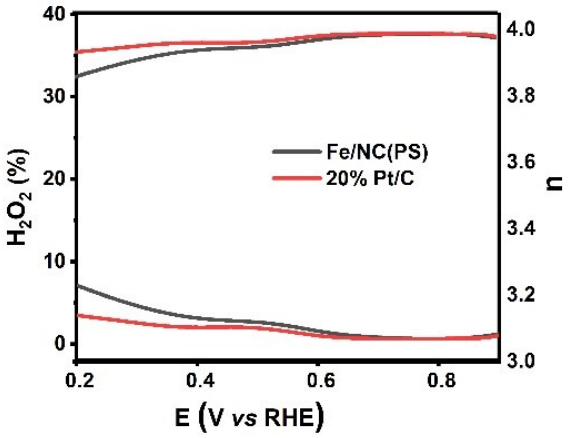

Fig. S17 Electron transfer number (*n*) and H_2O_2 yield of the Fe/NC(PS) and the commercial Pt/C.

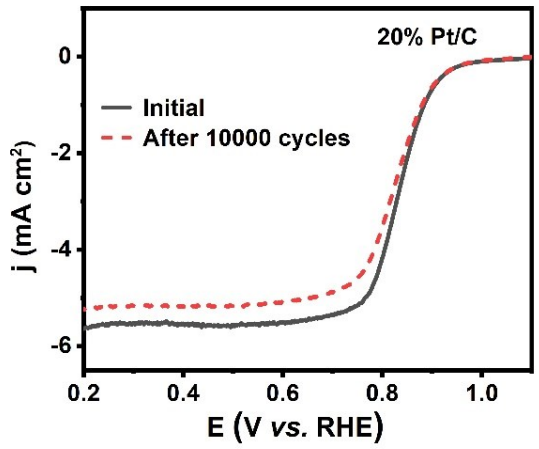

Fig. 18 ORR LSV curves for commercial Pt/C before and after 10000 cycles.

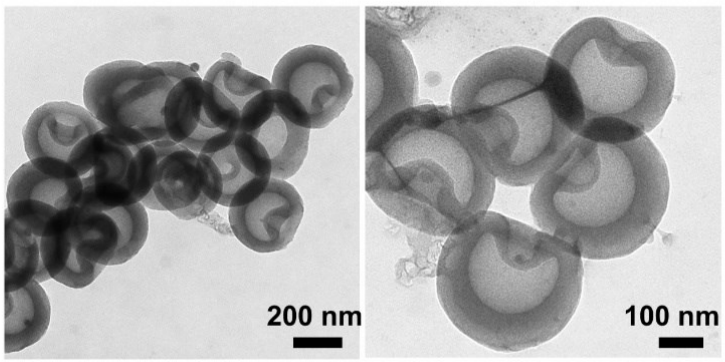

Fig. 19 TEM images of Fe/NC(PS) after 10000 cycles.

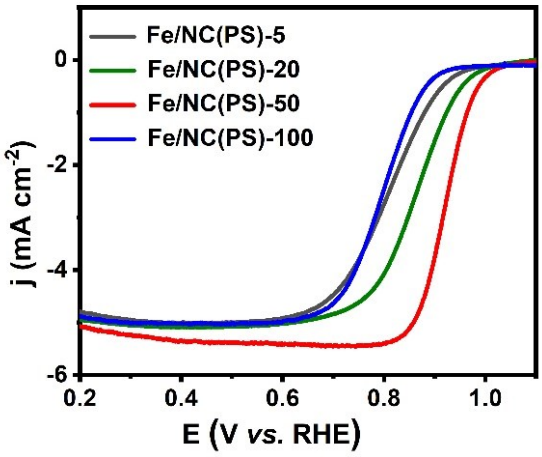

Fig. S20 LSV curves of Fe/NC(PS)–5, Fe/NC(PS)–20, Fe/NC(PS)–50 (also marked Fe/NC(PS)) and Fe/NC(PS)–100 in O_2–saturated 0.1 M KOH.

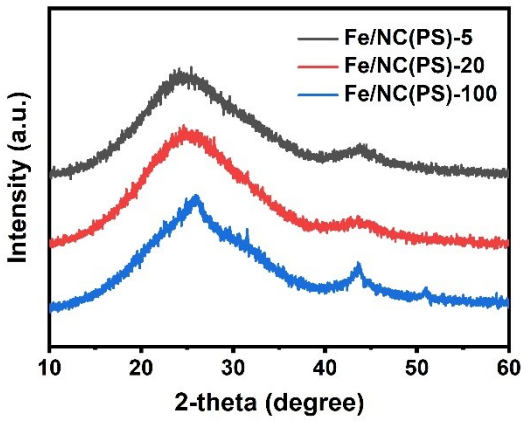

Fig. 21 XRD curves of Fe/NC(PS)–5, Fe/NC(PS)–20, and Fe/NC(PS)–100.

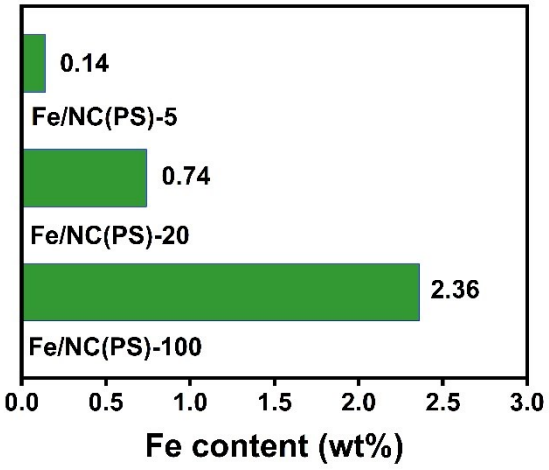

Fig. 22 ICP results of Fe/NC(PS)–5, Fe/NC(PS)–20, and Fe/NC(PS)–100.

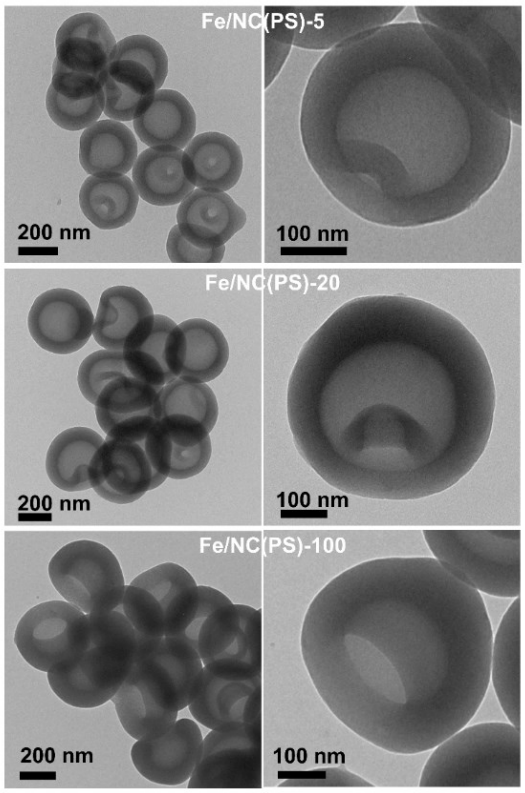

Fig. 23 TEM images of Fe/NC(PS)–5, Fe/NC(PS)–20, and Fe/NC(PS)–100.

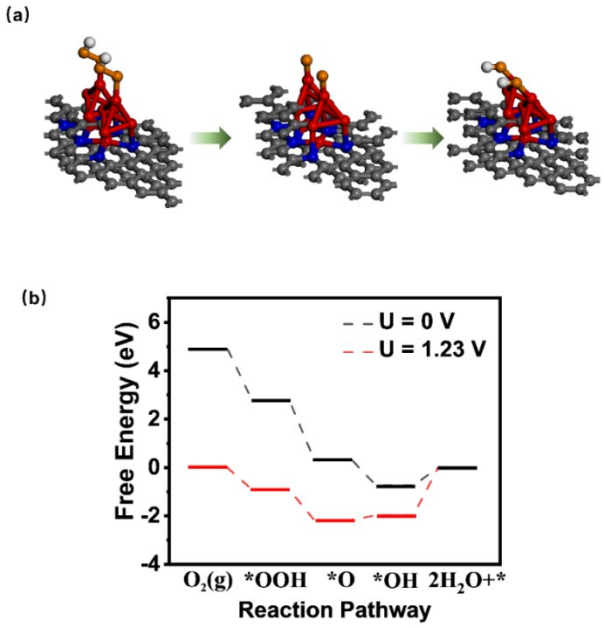

Fig. S24 (a) Structure of Fe_{NP}/C and the adsorption configurations of the ORR intermediates on the surface. (b) Free energy diagrams of ORR on Fe_{NP}/C.

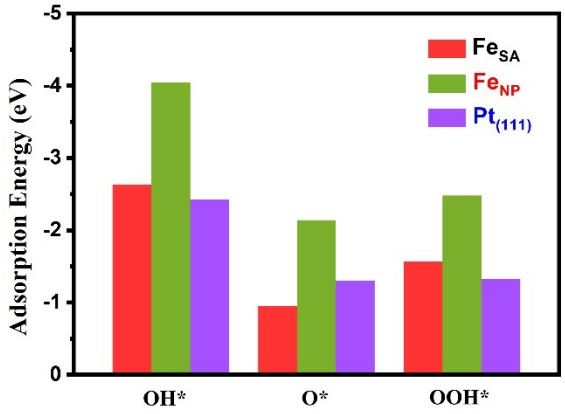

Fig. S25 Adsorption energies of the ORR intermediates on different catalytic sites.

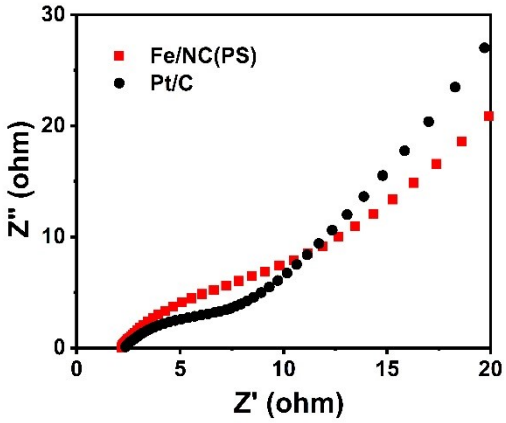

Fig. S26 Nyquist Curves of Zn-air batteries with different catalyst.

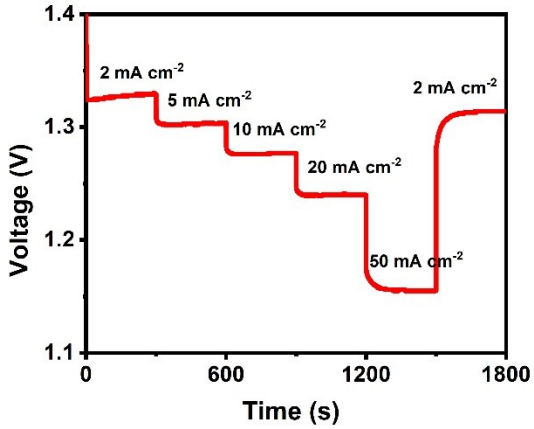

Fig. S27 Discharge curves of the zinc-air battery assembled with Fe/NC(PS) at current densities of 2, 5, 10, 20, 50, 2 mA cm^{-2}.

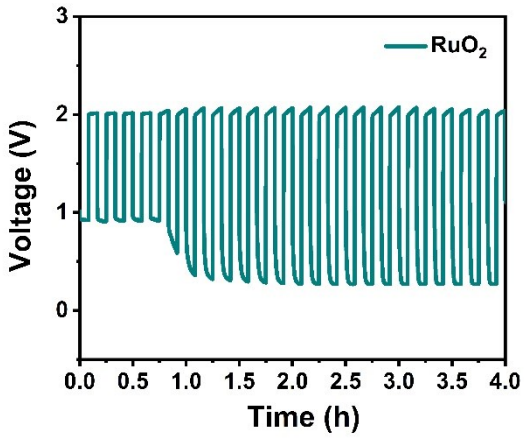

Fig. S28 The cycling curves of pure RuO2 as cathode for rechargeable Zn-air battery.

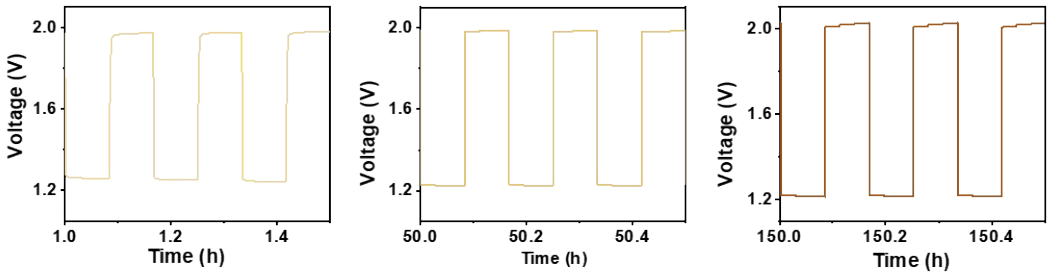

Fig. S29 The cycling curves at around 1h, 50 h and 150 h of rechargeable Zn–air battery with Fe/NC(PS)–RuO_2 and Zn foil as electrodes.

Table S1 Structural parameters extracted from the Fe K–edge EXAFS fitting.

sample	Scattering pair	CN	R(Å)	σ^2(10^{-3} Å^2)	ΔE_0(eV)	R factor
Fe/NC(PS)	Fe–N	4.4	2.12	3.4	16	0.07
Fe foil	Fe–Fe	6	2.45	4.5	5.14	0.007

Table S2. The Comparison of ORR performance of non–precious M/NC catalysts from the recent literature and this work (electrode 1600 rpm in 0.1 M KOH medium).

Catalysts	Half–wave potential	Onset potential (V vs RHE)	Electron transfer numbers	Reference
Fe/NC(PS)	0.919	1.03	4.02	***This work***
LDH@ZIF–67–800	0.83	0.94	4	*Adv. Mater. 2016,28, 2337*
Fe–N–CNFs	0.85	0.93	3.95	*Angew. Chem. Int. Ed. 2015, 54, 8179.*
Fe–N–SCCFs	0.883	1.03	3.9	*Nano Lett. 2017, 17, 2003.*
(Zn,Co)/NSC	0.893	1.07	3.9	*Nano Energy, 2019, 58, 277*
Co–N–C	0.881	0.982		*Angew.Chem. Int. Ed. 2016, 55*
Fe–N_4 SAs/NPC	0.885	0.972	3.84	*Angew.Chem.Int. Ed. 2018, 57,*
Fe SAs/N–G	0.92		3.95	*Adv. Mater. 2019, 31,*
Fe/OES	0.85	1		*Angew. Chem. Int. Ed. 2020, 59*
Fe–N_x–C	0.91	1.05	3.9	*Adv. Funct. Mater. 2019, 29*
Cu@Fe–N–C	0.896	1.01	4.0	*Adv. Funct. Mater. 2018, 28, 1802596*
Fe_3C–Co/NC	0.885		3.9	*Adv. Funct. Mater. 2019, 29*
	0.85	0.96	3.98	*Small 2018, 14, 1704319*
Co1-N3PS/HC	0.92	1.0	3.99	*Angew. Chem. Int. Ed. 2020, 59,2–12*
Co ISAs/GHSs	0.82		3.98	*Inorg. Chem. Front., 2020, 7, 3475–3481*

Table S3. Comparisons of the Fe/NC(PS) catalyst with other catalysts applied in Zn–air batteries

Catalysts	power density mW/cm²	Specific capacity mAh/$g_{(Zn)}$	Reference
Fe/NC(PS)	238	872	***This work***
CuS/NiS_2	172		*Adv. Funct. Mater. 2017, 27, 1703779*
FeNi@N–GR	85	765	*Adv. Funct. Mater. 2018, 28, 1706928*
NGM–Co	152	749	*Adv. Mater. 2017, 29, 1703185*
MnO/Co/PGC	172	873	*Adv. Mater. 2019, 31, 1902339*
Co/Co–N–C	132		*Adv. Mater. 2019, 31, 1901666*
NOGB	110		*Adv. Energy Mater. 2019, 9, 1803867*
Fe–N–C	202	800	*Adv. Energy Mater. 2019, 9, 1803046*
Fe/N–G	156	510	*Energy Technol. 2019, 7, 1900123*
Fe–NMG	218		*J. Power Sources 2018, 375, 214e221*
$CoO_x/CoN_y@CN_z$	204	1008.6	*Appl. Catal. B–Environ. 2020, 279, 119407*
CoSA/N,S-HCS	173	781	*Adv. Energy Mater. 2020, 2002896*
CoP/NP–HPC	186		*J. Mater. Chem. A 2020, 8, 19043–19049*
Pt–SCFP/C	122	790	*Adv. Energy Mater. 2020, 10, 1903271*
Ni/NiO nanosheet	225	853	*Nano-Micro Lett. 2020, 12, 68*
Fe–Co_4N@N–C	105	806	*Appl. Catal. B–Environ. 2019, 256, 117893*